UNITED NATIONS EDUCATIONAL, SCIENTIFIC AND CULTURAL ORGANIZATION
INTERNATIONAL CENTRE FOR THEORETICAL PHYSICS
I.C.T.P., P.O. BOX 586, 34100 TRIESTE, ITALY, CABLE: CENTRATOM TRIESTE

UNITED NATIONS INDUSTRIAL DEVELOPMENT ORGANIZATION

INTERNATIONAL CENTRE FOR SCIENCE AND HIGH TECHNOLOGY
c/o INTERNATIONAL CENTRE FOR THEORETICAL PHYSICS 34100 TRIESTE (ITALY) VIA GRIGNANO, 9 (ADRIATICO PALACE) P.O. BOX 586 TELEPHONE (040-224572 TELEFAX (040-224575 TELEX 460449 APH I

H4.SMR/540-7

Second Training College on Physics and Technology of Lasers and Optical Fibres

21 January - 15 February 1991

Delineation of Estuarine Fronts in the German-Bight using Airborne Laser-induced Water Raman Backscatter and Fluorescence of Water Column Constituents

Frank E. Hoge
NASA Goddard Space Flight Center
Wallops Island, Virginia, USA

INT. J. REMOTE SENSING, 1982, VOL. 3, NO. 4, 475–495

Delineation of estuarine fronts in the German Bight using airborne laser-induced water Raman backscatter and fluorescence of water column constituents

F. E. HOGE

NASA Wallops Flight Center, Wallops Island, Virginia 23337, U.S.A.

and R. N. SWIFT

E. G. & G. Washington Analytical Services Center, Inc., Pocomoke City, Maryland 21851, U.S.A.

(Received 5 February 1982; revision received 4 October 1982)

Abstract. The acquisition and application of airborne laser induced emission spectra from German Bight water during the 1979 MARSEN experiment is detailed for the synoptic location of estuarine fronts. The NASA Airborne Oceanographic Lidar (AOL) was operated in the fluorosensing mode. A nitrogen laser transmitter at 337·1 nm was used to stimulate the water column to obtain Gelbstoff or organic material fluorescence spectra together with water Raman backscatter. Maps showing the location and relative strength of estuarine fronts are presented. The distribution of the fronts indicates that mixing within the German Bight takes place across a relatively large area. Reasonable agreement between the patterns observed by the AOL and published results are obtained. The limitations and constraints of this technique are indicated and improvements to the AOL fluorosensor are discussed with respect to future ocean mapping applications.

1. Introduction

The NASA Wallops Flight Center (WFC) Airborne Oceanographic Lidar (AOL) participated in a total of seven flights during the 1979 Maritime Remote Sensing (MARSEN) experiment. In addition to the AOL, other NASA remote sensing instruments flown on the WFC P–3A aircraft included the Pulse Compression Altimeter (WFC), L&S Band Microwave Radiometer, and Dual Frequency Microwave Scatterometer (both Langley Research Center, LaRC). The AOL participation can be broadly separated into three categories: (*a*) ocean and estuarine front experiments (four missions), (*b*) ocean surface mapping experiments (two missions), and (*c*) ocean surface damping experiment (one mission). Only some results of the marine fronts investigations are presented here. The AOL support of ocean surface mapping for gravity wave spectral measurement has been given (Johnson *et al.* 1982). With the exception of the airborne laser portion, the ocean surface damping experiment is somewhat similar to those previously described (Huhnerfuss *et al.* 1978, 1981).

The overall MARSEN project was divided into two general areas, Ocean Fronts Experiments and Ocean Surface Experiments. The fronts experiments were to be conducted between 1 August and 15 September 1979, while the wave measurements were to be performed between 16 September and 31 October, 1979. The NASA remote sensing instruments onboard the WFC P–3A aircraft were each designed

0143–1161/82/0304 0475 $03·00

basically for participation in only one or other of these experiment types (with the exception of the AOL which can participate in both types), therefore, it was decided that the availability of the P–3A aircraft would span the latter portion of the fronts experiments and the beginning portion of the ocean surface wave measurement experiments. Due to unfortunate delays (both logistical and adverse weather) only two flight missions dedicated to observation of ocean fronts were performed during the fronts portion of the MARSEN project. This problem resulted in very limited overlap with related MARSEN experiments on the marine fronts.

2. Instrument description and configurations

During the marine fronts investigations the AOL was configured in a fluorosensing mode. Excitation was provided by a frequency doubled Nd:YAG laser (532·1 nm) on the missions flown on 17 and 18 September, while a nitrogen laser (337·1 nm) was utilized on the subsequent missions flown on 22 and 23 September. The preliminary results of the investigations conducted with the 532·1 nm laser have been published (Hoge and Swift 1981 a). Detailed discussions of the spectral response peaks obtained with pulsed laser sources have been presented by the authors (Hoge and Swift 1981 a, b) and by others (Bristow *et al.* 1981, Zimmerman *et al.* 1976). The results of the missions flown with the 337·1 nm nitrogen laser for the acquisition of Gelbstoff fluorescence have not been presented previously, however, other investigations utilizing this nitrogen laser source to measure tracer dye concentration (Hoge and Swift 1981 b) and oil slick thickness (Hoge and Swift 1980 a) have been given by the authors. Additional fluorosensor applications of the 337·1 nm nitrogen laser by others for oil fingerprinting tests and general fluorescence experiments have been published (Bristow 1978, O'Neil *et al.* 1980). Discussions of our results utilizing the 337·1 nm laser for the detection and mapping of frontal boundaries will be given herein.

In the fluorosensing mode, the Airborne Oceanographic Lidar (AOL) is a spatially, conically scanning laser-induced fluorosensor. The system possesses a real-time, multispectral, time-gated receiving capability. Thus, for each laser pulse transmitted into the ocean water column a complete fluorescence spectrum from 350 to 800 nm is recorded. The subsystems are designed to be very flexible thus allowing convenient adjustment in many transmitter and receiver optical settings as well as in electronic gate widths and delays. In addition, the optical table which accommodates the laser transmitter section allows for rapid change of lasers, filters, mirrors, etc.

2.1. *Ultraviolet laser system configuration*

The laser transmitter used during the missions flown on 22 and 23 September 1979 was an Avco model C–5000 pulsed nitrogen laser whose output wavelength is 337·1 nm. This laser produces pulses of ~ 100 kW peak power and 10 ns width. A high speed silicon photodiode on the rear of the laser provides the start pulse timing and the output power monitoring of the laser. Digitization and recording of this signal allows the received fluorescence and Raman data to be corrected for variations of laser output power. However, as will be seen, the water Raman backscatter signal can be utilized to provide an additional correction for laser power fluctuations. As shown in figure 1 the pulsed laser output is again folded through 90° in the horizontal plane of the upper tier into the adjustable beam divergence/collimating lens. The nitrogen laser output beam divergence can be controlled in the AOL system from 0·4 to 4 mrad. The minimum divergence was used during all of the present field

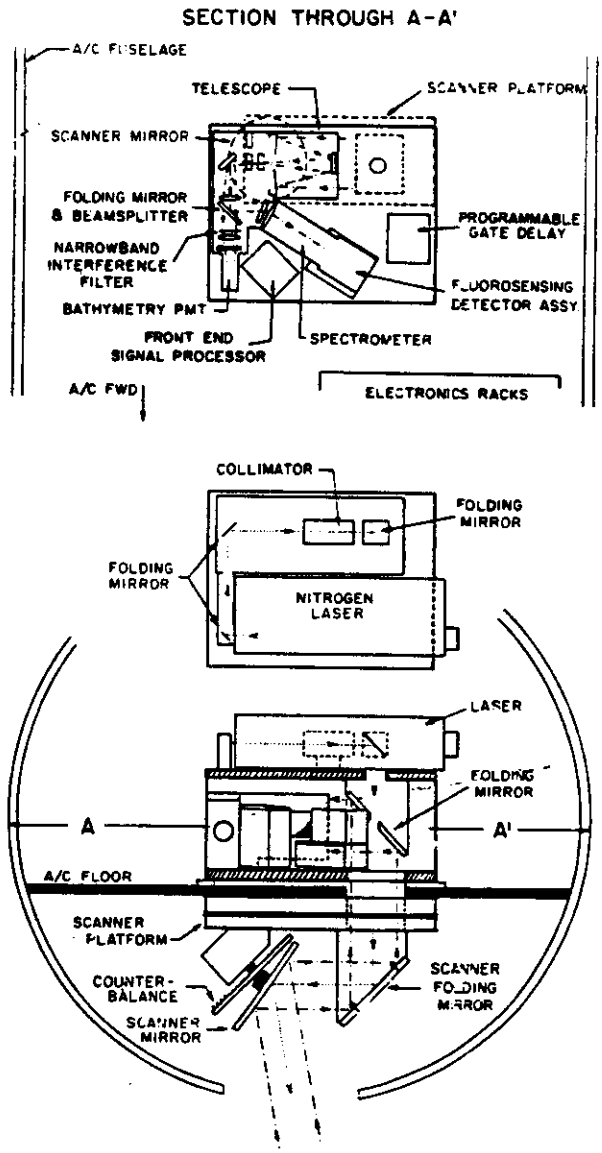

Figure 1. Elevation and plan view of the AOL illustrating three main optical tiers and selected optical components.

experiments. The beam is then folded downward, through the main receiver folding mirror, finally striking the angle adjustable, nutating scan mirror. The scan mirror is 56 cm in diameter and is connected at its centre in a wheel and axle type configuration. This mirror is integrally connected with an adjustable, concentric, counter-balance wheel so that the entire mechanism does not vibrate when the mirror is rotated in non-perpendicular positions of 5, 10, or 15°. All of the data reported in this paper were taken in a non-scanning profiling mode at a 5° off-nadir setting. This scan mirror finally directs the beam to the ocean surface. A cut-away illustration of the AOL system installed in the NASA P-3A aircraft is shown in figure 2. The total surface, volume, and ocean bottom backscattered signals return

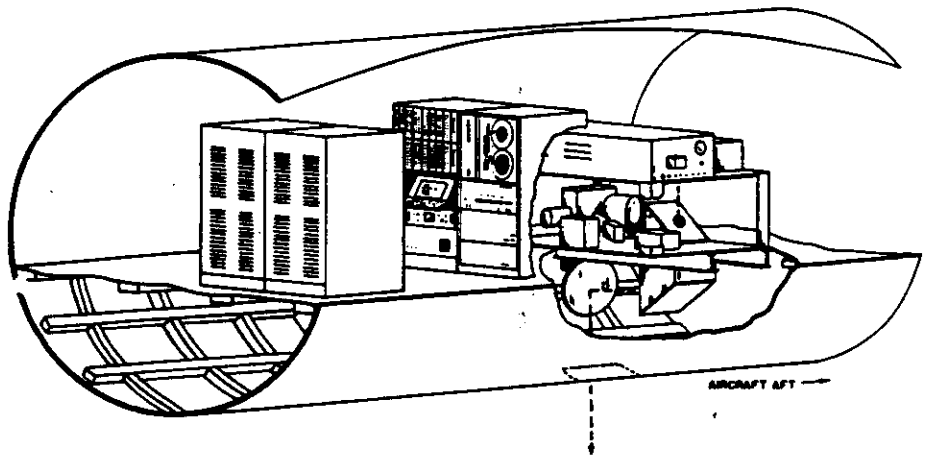

Figure 2. Cutaway illustration of the AOL installed in the NASA P–3 aircraft.

through the same path, but because of their uncollimated spatial extent are principally directed into the 30·5 cm Cassegrain receiving telescope located on the second optical tier. The horizontal and vertical fields of view of the receiving telescope are each separately controlled by a pair of operator adjustable focal plane knife edges. The radiation is then collimated to eliminate undesirable skewing of the bandpass by any subsequent narrow band interference filters. In this field experiment a Corning CS7–37 U.V. transmitting glass filter was used for background noise rejection. The radiation is then focused about 3 cm behind the face of an RCA 8575/2C PMT to minimize the influence of weak photocathode areas on the received signal. The combination 45° folding mirror and beam splitter located between the collimating lenses and the transmitting filter is used only in the fluorosensing mode. The beam splitting mirror directs a major portion of the laser excitation and fluorescent return signals into the fluorosensing detector assembly. The excitation wavelength (337·1 nm) component of the return signal is rejected from the spectrometer by a liquid filter consisting of a water solution of 2,7-dimethyl-3,6-diazcyclohepta-1, dieneperchlorate (Kasha 1948). This solution is a very effective filter that rejects radiation below ~340 nm. A small amount of the surface return signal is allowed to pass through a small (1-cm diameter) opening in the beam splitter where it is sensed by the bathymetry photomultiplier, and subsequently used to determine the slant range, and to generate the gate pulses for the analogue-to-digital charge digitizers (CD). The U.V. transmitting filter is placed into the 11 cm diameter collimated return beam just behind the beam splitter. The bathymetry portion of the system must function during all modes of operation and therefore precise slant range and/or altimetry information is available at all times.

The fluorosensing detection assembly contains an 11 cm diameter transmission diffraction grating blazed for 480 nm, having 600 grooves per millimetre. Figure 3 is a simple illustration of the fluorosensing spectrometer configuration used during these experiments. An 11 cm diameter simple lens brings the dispersed radiation to the entrance surface of 40 rigid, rectangular cross-section quartz light guides. These guides are optically coupled to two separate banks of 20 photomultiplier tubes. The short wavelength bank of tubes are RCA type 8644 while the remaining bank is an extended red type RCA C70042 version of the same tube. The front faces of the 40

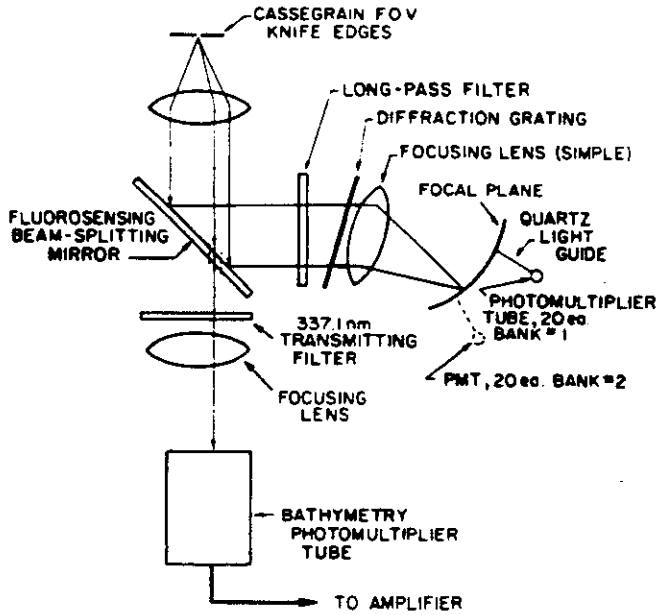

Figure 3. Principal components and layout of the 40-channel AOL spectrometer sybsystem.

light guides are physically located in the curved focal plane of the spectrometer to receive the dispersed spectral components nominally from 350 to 800 nm. This configuration thus yields a spectral bandwidth of approximately 11·25 nm for each channel. The tubes are not shuttered or gated but remain active at all times. Ambient background radiation rejection is provided by the 0 to 20 mrad adjustable FOV knife edge pairs located at the focal point of the receiving telescope. The optimum operational FOV for our field tests was experimentally determined to be 4 mrad by observing the OH – stretch water Raman SNR. The pulsed analogue outputs of the entire bank of phototubes are simultaneously routed to a.c. coupled buffer amplifiers that drive each of the 40 CD input channels. The amplifiers respond only to wide bandwidth fluorescent pulses thus minimizing background noise. For the laser fluorosensor data, all 40 CDs are gated on simultaneously at a temporal position determined by the surface return signal from the bathymetry photomultiplier tube. Forty separate delay cables from the PMT buffer amplifiers to the CDs allow a single channel switchable delay in the bathymetry mode to control the temporal position of the fluorosensor gates so as to correspond to points above, at, or below the ocean surface. The fluorosensing data acquisition mode is shown in figure 4.

Additionally, the CDs can be held 'on' for selectable integration times of 15, 50, or 150 ns using a LeCroy Model 620 discriminator. The CDs are, in effect, the analogue-to-digital converters for the AOL spectral waveform digitizing system. The CDs provide ten-bit resolution yielding a maximum of 1024 counts. The output from these digitizers is directed through standard CAMAC instrumentation to a Hewlett-Packard 21MX computer for recording. With proper delay adjustments relative to the bathymetry PMT derived surface return, the waveforms may be taken at any position above or below the ocean surface. In this experiment the spectral waveform data acquisition was started ~3 ns prior to encountering the surface and terminated ~40 ns later.

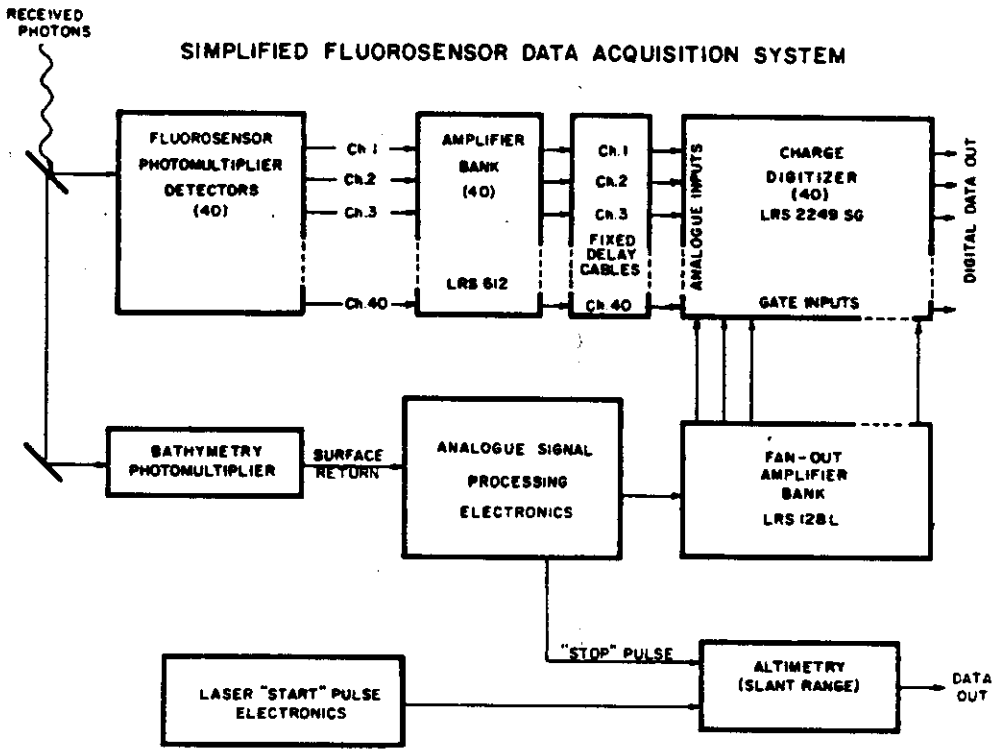

Figure 4. Basic AOL fluorosensor data acquisition subsystem.

3. Description of the study area

Marine fronts are boundaries between watermasses of differing chemical, biological, or physical properties. The importance of these features in the dynamics governing exchanges between watermasses has been stressed in a number of recent publications. Likewise the potential for magnification of various entrained constituents in convergence zones associated with many marine fronts has been recognized (Klemas and Polis 1977, Bowman and Esaias 1978). The development, stability, and dissipation of fronts within estuaries such as the German Bight is especially fundamental to the understanding of processes within those watermasses.

The inflow of freshet and saline marine water into an estuary serve to maintain a potential for density contrasts. Thermal differences within estuaries can have the effect of increasing or decreasing these density contrasts. In mid-latitude estuaries such as the German Bight the inflow from fresh water sources tends to be warmer in the summer than water from marine sources thus adding to the density differences. Conversely, during late fall and early winter the fresh water inflow may be colder than the water from marine sources effectively reducing the density differences. Tides and wind as well as the shape and depth of the estuary all affect mixing characteristics including the formation and strength of fronts.

The German Bight region of the North Sea shown in figure 5 is a roughly 'funnel' shaped embayment bordering the German coastline. Estuarine conditions are sustained primarily by inflow of freshet from the Elbe and Weser Rivers which both empty into the bight near the apex. The depth is generally in excess of 20 m over most of the central and southern portions as indicated by the 20 m contour in figure

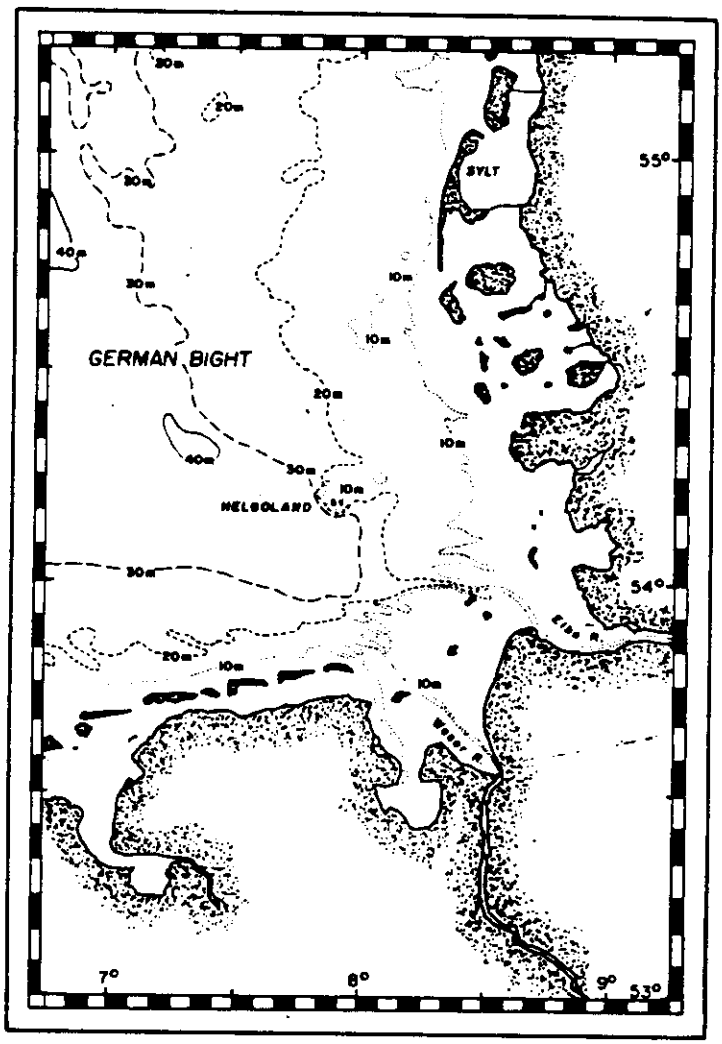

Figure 5. Bathymetry of German Bight.

5 while the eastern section is generally shallower than 10 m. Large mud flats fringe most of the landward edges of the bight. The fossil channel of the Elbe River can be seen cutting the estuarine floor effectively bisecting the inner bight region. Recently published surveys indicate that the deeper channel acts as a conduit for the intrusion of the denser marine bottom water into the inner estuary.

Residual currents within the bight largely parallel the coast. This results in the movement of higher salinity marine water from the North Sea into the bight from the west and a drift of fresher estuarine water out of the bight to the north. The area of greatest mixing for the fresh water inflow is in the area north and west of the mouth of the Elbe River where the strongest salinity gradients were reported in studies performed both in 1976 (Becker *et al.* 1979) and 1979 (Becker and Prahm-Rodewald 1980). Becker and Prahm-Rodewald (1980) reported surface salinity gradients of up to 0·4 parts per thousand per 100 m in this region and a total salinity

change across a single strong front of 4 parts per thousand accompanied by a temperature change of less than 1°C.

The presence of fronts within the German Bight have been known for some time. Measurements conducted during the 1960s and earlier using classical techniques established the presence of the large mixing zone west and north of the mouth of the Elbe River. More recent observations, some conducted with continuous recording equipment in the near surface layer and sensors towed on depth controllable fish, have revealed that the mixing zone is composed of a series of smaller fronts. As we shall see our airborne results corroborate the presence of many small fronts.

During a MARSEN survey conducted with the German research vessels *Gauss* and *Frederick Heincke* in the month preceding the AOL missions the fronts were shown to be aligned in an echelon fashion trending SE. to NNW. Both the position and intensity of these individual fronts change with time, however the zone itself appears to be temporally stable (Becker and Prahm-Rodewald 1980).

4. Scientific setting

The study of fronts in coastal watermasses is currently hampered by various sampling problems which must be resolved before the dynamics of mixing can be understood. Major advances in *in situ* sampling equipment in recent years has enabled the oceanographer to collect continuous surface and, to some degree, subsurface observations along a cruise track. For many purposes these increased capabilities appear to be sufficient. Major vertical and horizontal gradients of large water bodies can be adequately mapped. Further, interesting observations of the dynamics involved in the mixing at boundaries between these watermasses have been provided by various eulerian and lagrangian methods of sampling. Despite these advances the understanding of frontal boundaries from ship gathered data remains essentially two-dimensional since the synopticity of the ship data is severely limited by the relatively low speeds of the vessels.

Likewise, the remote sensing of coastal watermasses from airborne and spaceborne platforms have had inherent problems. A persistant problem has been the lack of precision and accuracy in the measurements taken by these sensors which are still in their relative infancy. Recently, reported results from experiments conducted by various researchers suggest that this difficulty is starting to be resolved for a number of sensors, at least in the near surface layer (Bristow *et al.* 1981, Swift 1980, Blume *et al.* 1981, O'Neil *et al.* 1981). Observations made from satellites are essentially synoptic, can be made with repeated passes over long periods of time, and are relatively inexpensive considering the volume of data that can be collected. Although showing improved accuracy (Gordon 1981) the spaceborne sensors are still constrained to orbital schedules, and many sensors operating in the visible spectral region are hampered by cloud cover. In certain regions such as the North Sea a persistent cloud cover precludes the likelihood of acquiring successive data sets necessary for a number of disciplines involved in studying frontal processes.

Airborne sensors are able to acquire high rate data, can operate in shallow waters not accessible by ships, can generally be scheduled when and as needed, are usually somewhat more accurate than their spaceborne counterparts, atmospheric effects are significantly reduced, and certain of these sensors are only available for aircraft platforms. Observations by airborne optical sensors are similarly affected by cloud cover, however, flexibility in scheduling and selection of altitude affords the airborne optical sensors a considerably improved opportunity for making measurements. The

airborne data can, in a practical sense be considered nearly synoptic over intermediate size bodies of water such as the German Bight although the relative movement of the watermass during the course of a mission cannot be totally ignored. The airborne sensors can on the other hand, be more expensive to operate if a large volume of data is required and/or if the transit distance is large.

Remote sensors operating in the microwave spectral regions are especially confined to observations of only the water surface. Optical sensors are, on the other hand, able to obtain signals from the ocean volume over much of the visible spectrum. Passive optical sensors necessarily get an integrated signal from the water column and for the most part active lidar fluorosensing systems have confined observations to the integration of signal from the upper 5 to 10 m (O'Neil *et al.* 1981). Several airborne lidars have however demonstrated the capability of temporally sampling the on-frequency pulsed laser return to extract water depth in laser bathymetry experiments (Hoge *et al.* 1980, Penny and Philips 1981, O'Neil 1981). The AOL does have the capability of delaying the integration of the return spectral fluorescent signal and can selectively set the integration period between 4 and 150 ns. Thus, on successive passes different layers below the ocean surface could be mapped. Alternatively, temporally sampled (and thus depth resolved) water Raman backscattered waveforms (unpublished) have recently been obtained with the AOL utilizing a narrow band interference filter in front of the bathymetry PMT centred on the Raman shifted wavelength. By utilizing selected narrow band filters this technique could be used on repeated passes to assess the vertical distribution of various fluorescing constituents in the water column.

Despite the potential availability of airborne depth resolved measurements from airborne lidar systems, detailed work in estuarine frontal systems will, for the foreseeable future, be best addressed from combinations of airborne and *in situ* sensors. Rather severe attenuation of laser and fluorescence signal due to high sediment loads normally entrained in estuarine waterbodies precludes taking measurements from very deep into the water column. This is especially true in the 680 to 685 nm spectral region where chlorophyll *a* fluorescenses. In addition, the lack of supportive physical measurements below the surface layer for airborne sensors requires subsurface measurements from shipborne instrumentation for best quantification and interpretation of the optical observations.

5. Description of the experiment

The 337·1 nm pulsed nitrogen laser was operated at various repetition rates during these experiments. Although capable of acquiring 400 pps fluorosensing data with this laser, the AOL was operated primarily at 50 pps to reduce the high volume of data. On shorter flightlines and where higher horizontal spatial variation was expected the system was operated at 100 or 200 pps. Figure 6 (a) shows a laboratory spectrum obtained from a Chesapeake Bay water sample when stimulated with a 337·1 nm nitrogen laser in our Wallops Flight Center laser laboratory. This spectrum is considered typical of estuarine water bodies. As one moves to deeper, open ocean areas the amount of dissolved organic fluorescence generally declines to levels approaching those found in distilled, deionized water (Hoge and Swift 1981 b). The laboratory laser spectrofluorometer arrangement used to obtain this data was similar to one already described (Hoge and Swift 1981 b). Spectra obtained with the AOL from more turbid, nearshore and clearer, offshore waters of the German Bight are contrasted in figure 6 (*b*) and (*c*) respectively. A vertical scale in raw counts from the

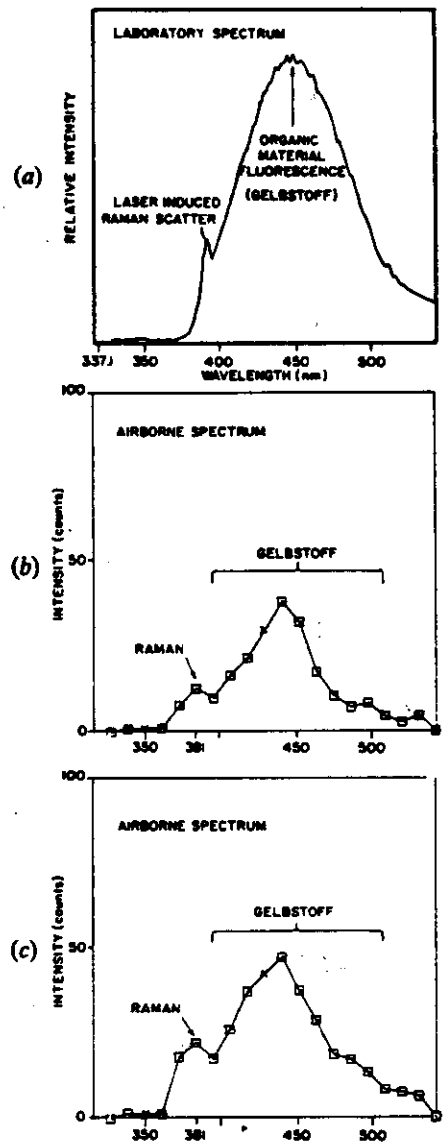

Figure 6. Laser induced fluorescence spectra from estuarine watermasses.

fluorosensor digitizer has been used in figure 6(*b*) and (*c*) as well as in subsequent figures for comparative purposes. The spatial positions of these samples within the German Bight are shown in figure 7(*a*) as 'S1' and 'S2' respectively. Certain of the fluorosensor channels which were not operational during these experiments are indicated with 'X's on figures 6(*b*) and (*c*). Note the Raman backscatter line centred at 381 nm and the broad Gelbstoff fluorescent response are labelled on both the laboratory and airborne spectra. Each airborne spectrum has been corrected for variations in both laser power and altitude and is an average of 50 separate waveforms taken over a distance of 100 m. The small amount of Gelbstoff fluorescence in the Raman band has not been removed from the spectra in the figure 6 plots. Thus, the ultimate effect will be relative Raman levels that are slightly high in

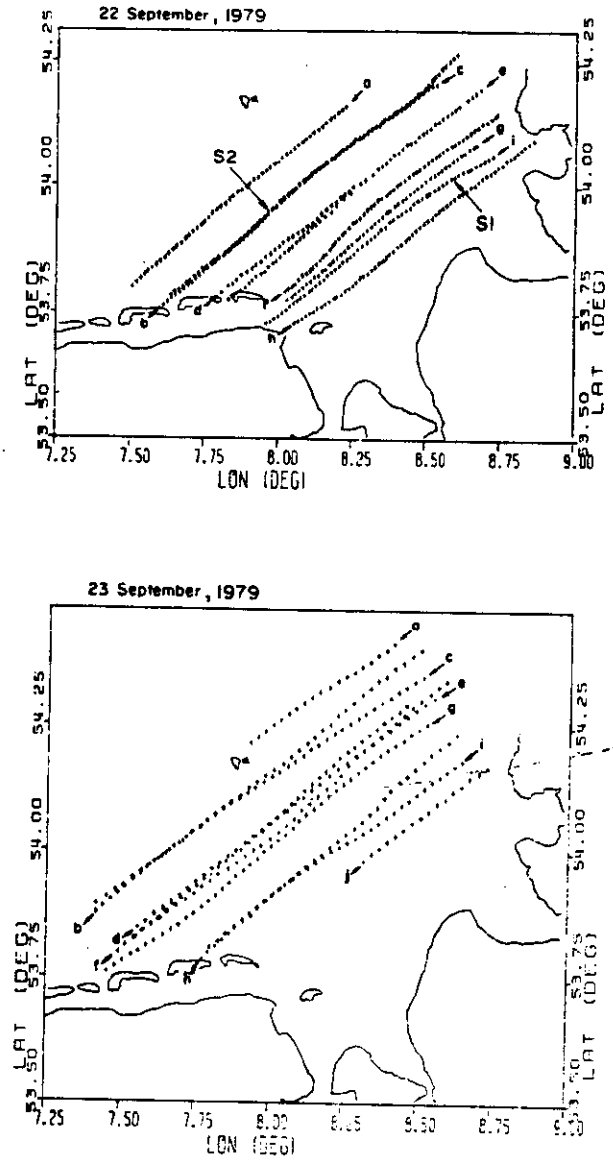

Figure 7. Maps of the AOL profiling passes for missions flown on 22 and 63 September 1979.

the inner portion of the Bight where Gelbstoff fluorescence has reached significant proportions at the 381 nm Raman line. Following the normalization procedure described later in this text the nearshore relative Gelbstoff levels will be slightly low. Background fluorescence at the same wavelength as the Raman band can be removed using well-known interpolation techniques (Hoge and Swift 1980a, Kung and Itzkan 1976). Unfortunately, at the time of the MARSEN experiments dependable calibration between individual fluorosensor channels was not available, therefore no interpolation was attempted in this initial data set. As indicated previously the laser wavelength has been rejected from the spectrometer with a bulk volume chemical liquid filter. No corrections have been made to our data for this

filter since only minor effects occur in those channels used for our frontal boundary detection. As shall be seen, these spectral resolution problems have no significant effect on the overall detection and mapping of estuarine fronts. However, we should emphasize that for other specific applications of the Raman backscatter signal, such as the measurement of oil film thickness, dye concentration, and water optical transmission, the unwanted fluorescence contributions must be removed.

The flightlines occupied on the 22 and 23 September 1979 missions are shown in figure 7 (*a*) and (*b*) respectively. Considerable overlap in certain of the flightlines is apparent on both maps. The overlap was intentionally provided in order to support some of the other sensors operating simultaneously onboard the P–3A aircraft during these estuarine front mapping missions. Although such overlap does not effectively utilize the potential spatial coverage of an airborne sensor it does afford an opportunity for checking the reproducibility and internal consistency of remote sensors still in the developmental stage, especially when no surface truthing is available. This aspect will be subsequently discussed.

Figure 8 shows profile data from the SW portion of flightline 'f' from figure 7 (*b*) plotted against time for the Raman backscatter peak channel (6) and a channel (11) from the broad Gelbstoff fluorescence return. Figure 8 will serve to illustrate several aspects of our data processing and interpretation. The data have been averaged over a 2-s period in order to reduce the number of points to be plotted. The number of points used in this simple average varied from 100 to 400 points depending on the laser repetition and sampling rates. Flightline 'f' was obtained at 50 pps, consequently the plotted mean values were each determined from 100 points. Subsequently these simple, 2-s averages were further filtered with a seven point moving average to reduce the higher frequency fluctuations in the data so that the major features in the profile such as estuarine fronts would become accented. The water Raman profile is presented in figure 8 (*a*). An increase in the Raman signal indicates that the total integrated water column has a higher transmission at the laser excitation wavelength 337·1 nm and at the Raman emission wavelength of 381 nm. Similarly, a decrease in the Raman backscatter strength should be interpreted as a decrease in the water column optical transmission at the above wavelengths (Swift and Hoge 1981 b). It can be shown (Bristow *et al.* 1981, Hoge and Swift 1981 b, Kung and Itzkan 1976) that the Raman backscatter signal strength is inversely proportional to the sum of the extinction coefficients of the water column at the laser and Raman emission wavelengths respectively.

Figure 8 (*b*) is a profile of the Gelbstoff fluorescence. The observed amplitude of the Gelbstoff response is a product of both the concentration of fluorescing, dissolved organic material and the optical transmissivity of the water column. In a clear, homogeneous watermass the same concentration of fluorescing dissolved organic compounds would yield a higher Gelbstoff response signal from a laser pulse than would be obtained in turbid water simply because the laser beam has accessed a larger volume of water and therefore more of the dissolved organic material. The dominant effect of changes in water optical transmission properties becomes readily apparent when the Raman and Gelbstoff profiles are compared (figure 8 (*a*) and 8 (*b*) respectively). Notice, for the most part, that inflexions in the Raman profile are reflected in the Gelbstoff profile. Although the sense of movement is generally the same in both profile traces, the degree of the corresponding movement is quite variable at certain points designated '1 to 5' on figure 8 (*a*) and (*b*). Normalization of the fluorescence signal with the Raman backscatter signal significantly reduces the

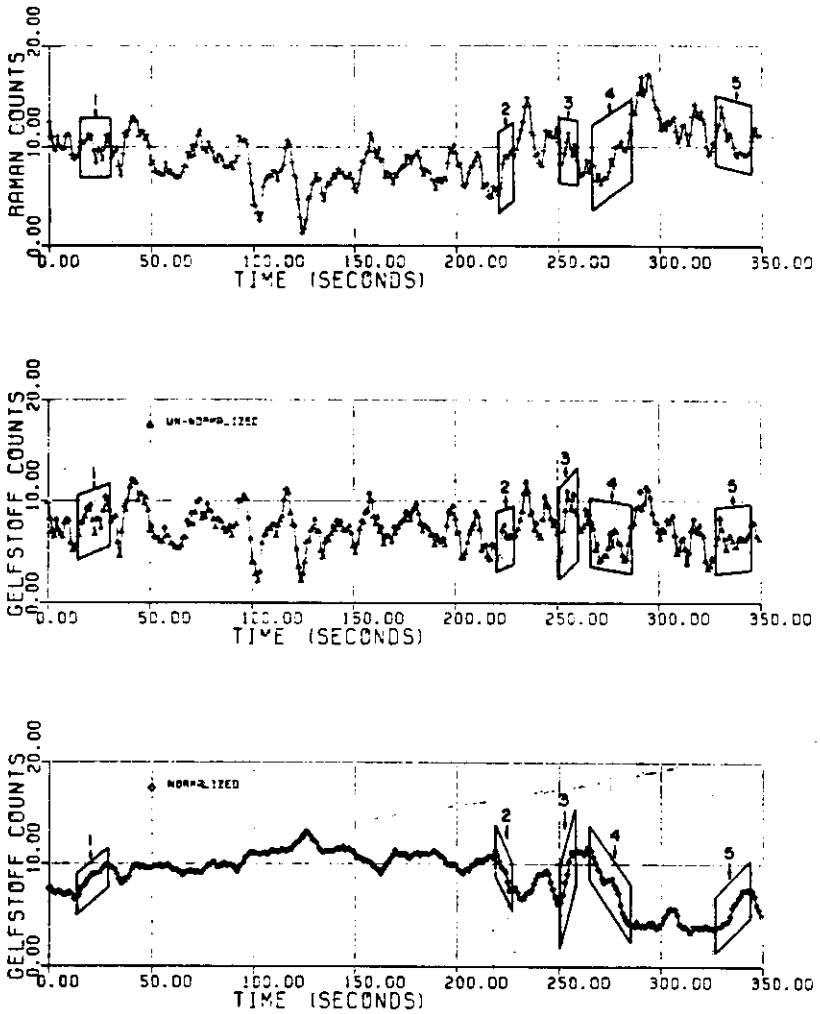

Figure 8. Profiles of Raman backscatter as well as unnormalized and normalized Gelbstoff fluorescence from the SW. portion of flightline 'f' of figure 7 (*b*).

effect of these changes in water optical transmission properties on the corrected fluorescence signal. This technique has been previously discussed in more detail in connection with other AOL applications (Hoge and Swift 1981 a; Hoge and Swift 1981 b). Figure 8 (*c*) is the corrected Gelbstoff fluorescence signal. Notice that the amplitude remains reasonably smooth over most of the flightline except at the points indicated by the numbers '1 to 5' where significant changes in the corrected Gelbstoff occur. Flightlines located in the inner portion of the bight were much less dominated by the Raman backscattered signal, frequently showing an opposite sense of movement between the raw Raman and Gelbstoff signals resulting in correspondingly larger fluctuations in the normalized Gelbstoff fluorescence amplitude. It is worth noting that a multichannel fluorosensor is required to correct the fluorescence signal for changes in water clarity.

The overlap in flightlines from the two missions provides a number of opportunities to compare data between passes as previously mentioned. Figure 9

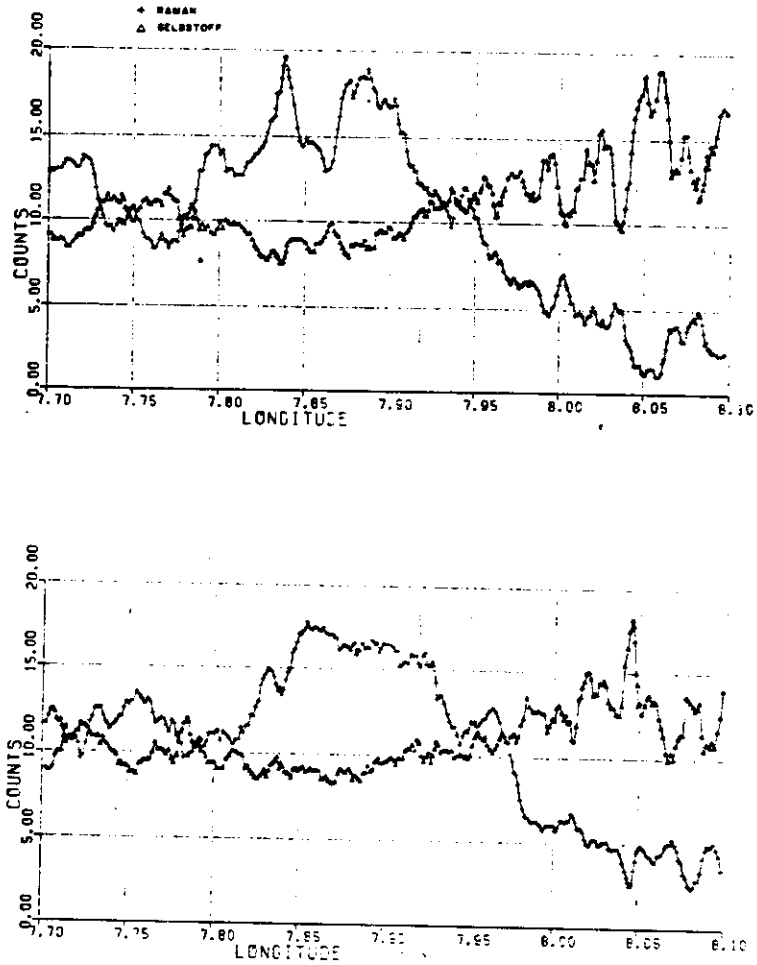

Figure 9. Comparative profile cross-sections of the overlapping portions of flightlines 'b' and 'c' from figure 7(*a*).

shows comparative profile data of Raman backscatter and normalized Gelbstoff fluorescence plotted against longitude from the overlapping portion of flightlines 'b' and 'c' (figure 7(*a*)). These passes were flown in the opposite direction from each other as indicated on figure 7(*a*). The observations between the two passes were separated by approximately 20 min. Despite the temporal difference and some spatial uncertainties in relative position considerable agreement can be seen between the profiles from the two passes in both Raman backscatter and normalized Gelbstoff fluorescence. Other overlapping flightline segments in the outer portion of the bight compared well even for relatively small detail as is evidenced in figure 9. However, overlapping flightline segments from the inner portion of the bight did not compare as favourably. The gross features in the latter data sets could be discerned in the separate profiles taken over the same ground track, but finer detail (<5 km) generally did not agree. Perhaps this lack of agreement can be attributed for the most part to the higher dynamic conditions of mixing and resuspension that occur within the shoaler bathymetric framework. Distribution patterns of both turbidity and dissolved organic matter in the inner bight are considerably smaller in spatial extent

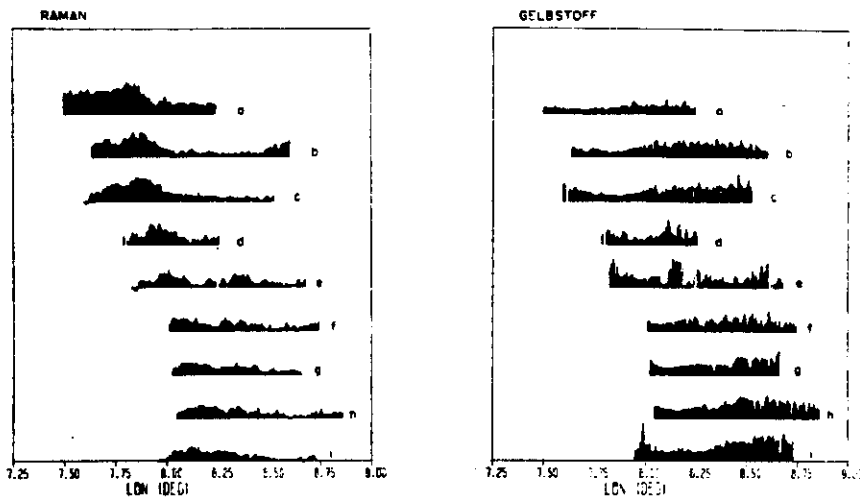

Figure 10. 'Stick' profiles of Raman backscatter and Gelbstoff fluorescence from 22 September 1979.

and are more irregular. Thus relatively small differences in position between passes can result in quite different observations.

Figures 10 and 11 are 'stick' profiles of Raman and normalized Gelbstoff signal for all of the passes obtained on the missions flown on 22 and 23 September 1979. The vertical scale of the profiles is 200 counts per centimetre and the horizontal scale is plotted in degrees of longitude to facilitate comparison of the flightlines which were flown alternately in opposite direction from one another as was indicated in figure 7. Some care must be exercised in making data comparisons between the diagrams from the 22 September mission with those from the 23 September mission. As can be seen in figure 7, corresponding flightlines flown on 23 September were

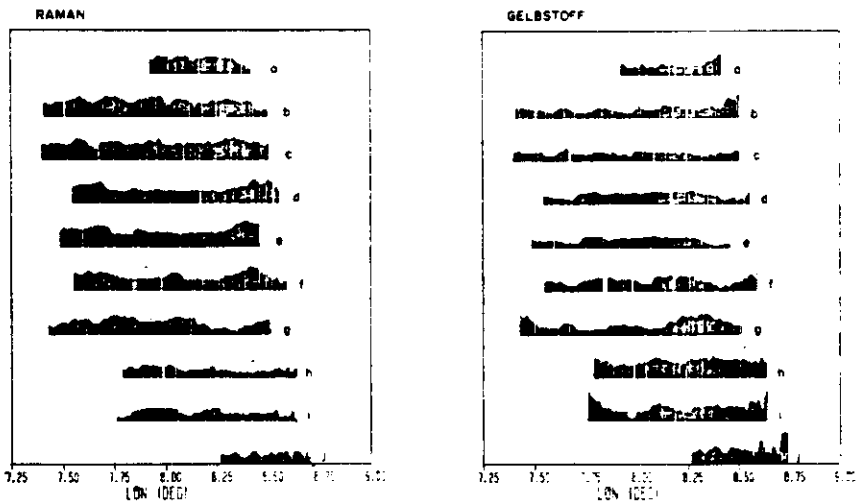

Figure 11. 'Stick' profiles of Raman backscatter and Gelbstoff fluorescence from 23 September 1979.

offset seaward of those flown on 22 September. Therefore profile 'j' from figure 11 is at approximately the same distance offshore as profile 'e' in figure 10.

The 'stick' diagrams given in figures 10 and 11, coupled with the flightline ground tracks in figure 7, permit an assessment of the general distribution of turbidity and fluorescing, dissolved organic matter within the German Bight on 22 and 23 September 1979. The inner bight and eastern side of the bight can be characterized as having high sediment and dissolved organic concentrations while the outer portion of the bight is comparatively low in both sediment and dissolved organic load. This perspective can be improved somewhat by contouring the data as shown in figure 12 for the mission flown on 22 September 1979. The diagrams as well as the contoured

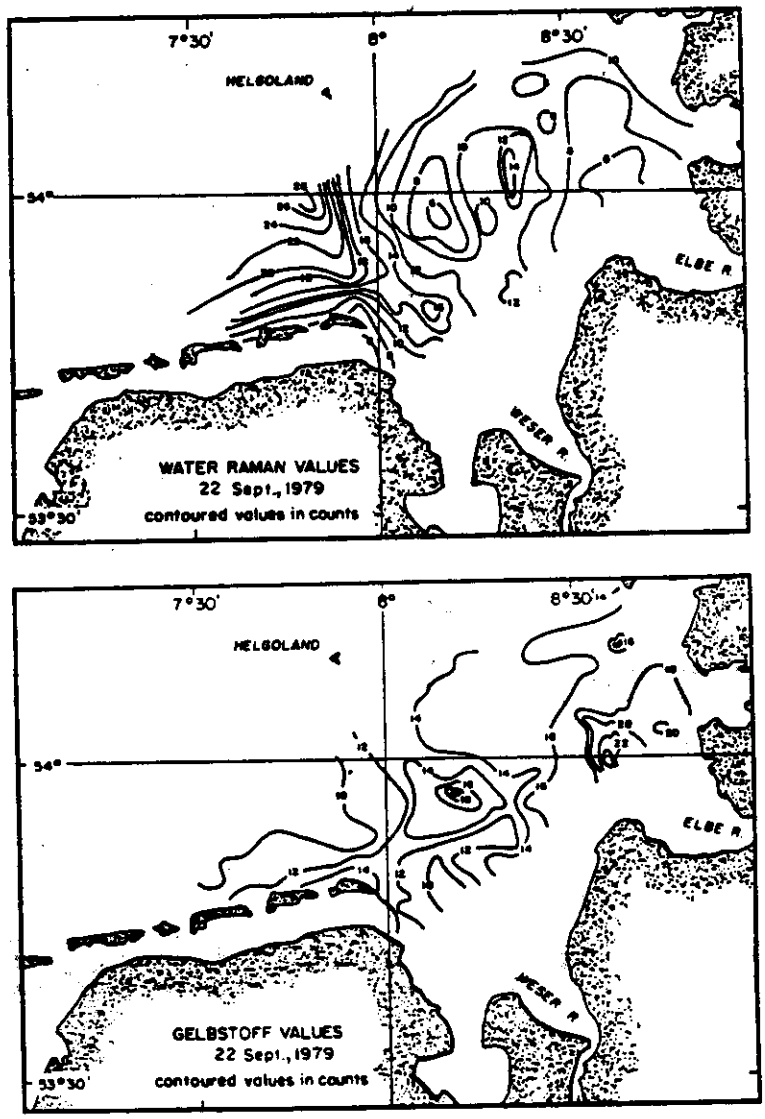

Figure 12. Contoured plots of water Raman backscatter and normalized Gelbstoff fluorescence for the mission flown on 22 September 1979.

projections of the data indicate that these two distinct water bodies within the bight are separated by a large mixing zone located north and west of the Elbe River. Exchanges within this zone appear to be taking place along many smaller fronts rather than along a single large, front. Cells of water often in excess of 5 km across appear to have separated from both of the distinct water bodies and to have become distributed throughout the mixing zone. From the airborne lidar observations these cells, together with the frontal boundaries associated with them, can be discerned by changes in both water Raman backscatter and Gelbstoff fluorescence. These fluctuations are apparent in the expanded or detailed profiles from figures 8 and 9 and can be seen to some extent on the 'stick' diagrams in figures 10 and 11.

The general distribution of the watermass within the German Bight interpreted from the AOL fluorosensing data is in fair agreement with results published by German scientists based on earlier shipboard observations (Becker *et al.* 1979) and with shipboard observations conducted approximately 1 month prior to our MARSEN flights (Becker and Prahm-Rodewald 1980, I. James 1981, personal communication). In addition these patterns indicate a net transport of water within the bight consistent with the mean surface current vectors from HF radar measurements taken during the time frame covered by our observations (Janopaul *et al.* 1981). The degree to which Raman backscatter and Gelbstoff fluorescence can be used to tag watermasses is somewhat in question. Certainly neither parameter can be considered conservative enough for universal application as a tag. The Raman backscatter which is a measure of the attenuation properties of the upper water column is especially susceptible to local variation due to resuspension of bottom materials, phytoplankton blooms, and surface films. Gelbstoff fluorescence is somewhat better suited as a tracer of watermass movement, particularly in relatively small embayments such as the German Bight where source areas are both limited and identifiable. Some minor ambiquity in interpretation may arise, however, from small marine contributing sources and sinks of dissolved organic substances and from other fluorescent sources within the Gelbstoff spectral region. It is therefore suggested that this approach may be limited to qualitative estimations and not to models which require rigorous quantification of input data unless some surface observations are available to ensure the reliability of the airborne Gelbstoff measurements.

Cognizant of the above limitations and constraints, we attempted to utilize the profile data from the two experiments to assess the potential capability of an airborne lidar system for providing synoptic maps of marine fronts in estuarine areas. This analysis centred on the identification of boundaries between the offshore marine water and the nearshore water which was strongly influenced by terrestrial contributions largely from the Elbe and Weser Rivers. The Raman backscatter signal was used only to normalize the Gelbstoff fluorescence signal in order to correct for spatial variations in the attenuation properties of the German Bight. Changes in the water character due to sediment plumes and plankton blooms were thus removed or at least substantially reduced.

Maps of the German Bight on to which the major fronts have been projected for missions flown on 22 and 23 September 1979 are given in figure 13(*a*) and (*b*) respectively. The locations of the fronts are shown by the symbol located at the base of each line on the map. The length of each line is proportional to the relative strength of the front in units of counts of change/km. A 1 cm line represents a change in normalized Gelbstoff fluorescence of 50 counts/km. The relative direction of the

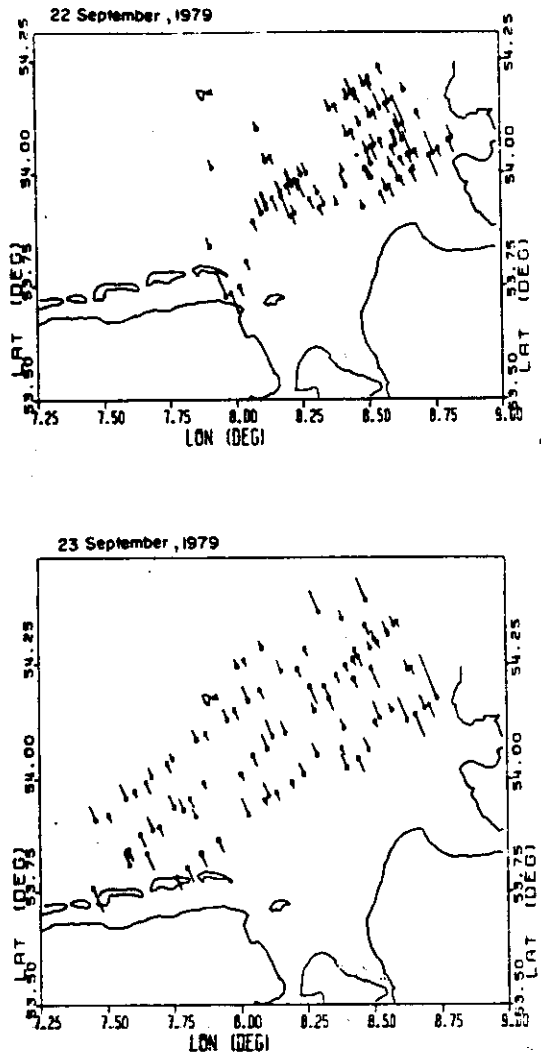

Figure 13. Maps indicating the major frontal features in the German Bight for 22 and 23 September 1979.

individual lines indicates the sense of the change in Gelbstoff fluorescence relative to the flight line as encountered moving from SW. to NE. irrespective of the original flight direction. For example, if the Gelbstoff fluorescence level increased, the line points away from the symbol and extends to the NW. and conversely decreased fluorescence is indicated by a line extending away from the symbol to the SE. The arbitrary selection of processing direction along the flightlines from SW. to NE. was done in order to avoid ambiguity in the interpretation of the slope of the fluorescent profile at each of the fronts along passes occupied in opposite direction from one another. For instance on a pass flown from SW. to NE. an increase in Gelbstoff fluorescence would be seen as positive, but the same front when approached on a path flown from NE. to SW. would have been viewed as negative.

An arbitrary cut-off was used in the selection of fronts to be displayed on these

composites in order to separate the major boundary features from the large number of lesser perturbations in the normalized Gelbstoff fluorescence return profiles. As an example, the frontal features selected from flightline 'f' are indicated by the numbers '1 to 5' on figure 8(*c*).

The composites shown on figure 13(*a*) and (*b*) indicate that frontal features associated with the mixing of marine and estuarine watermasses can be found throughout the inner bight region with the highest concentrations located both north of the Elbe River and northwest of the Weser River. Further, the formation of these fronts persisted seaward into the bight at least as far as Helgoland, the furthest extent of our areal coverage. The strongest fronts were located near the southern and eastern extremities of the inner bight where the rate of bathymetric shoaling reaches a maximum. Unfortunately, the interpretation of frontal density from these composites is somewhat misleading due to the oddly spaced and often overlapping flightlines and because, although the relative strengths of the frontal features are conveyed in the composite, the amount of fluorescence on both sides of a front cannot be determined directly. This latter problem can be aided somewhat by referring to the appropriate 'stick' diagrams in figures 10(*b*) and 11(*b*) and to the contoured projections presented in figure 12.

The distribution patterns of the fronts as determined from the AOL fluorosensing data are essentially constrained to a SW./NW. view. Unfortunately no passes were flown from which we could examine the spatial extent and relative strength of the individual fronts in a direction normal to the flight paths presented in figure 7. As can be seen in the composite frontal diagrams given in figure 13, the placement and sense of slope of Gelbstoff fluorescence across the fronts did not agree well enough between flightlines, which were spaced in some cases 10 to 15 km apart, to allow connection with any degree of certainty. Our synoptic airborne data cannot therefore yield any quantitative estimate of the extent of the water cells within the mixing zone in the NW./SE. direction. This would suggest that a more optimum flight grid be established for future airborne missions in the Bight. A comparison between these frontal composites and those recently published from earlier MARSEN experiments based on data gathered by German oceanographers (Becker and Prahm-Rodewald 1980) is difficult. The German data were not obtained in a synoptic fashion and were largely confined to the deeper, outer portion of the bight. Almost all of their observations were made seaward of Helgoland and in water depths primarily in excess of 20 m but in no cases shoaler than 10 m. Additionally, during the intervening month between the shipborne and airborne data sets the basic stratification structure within the bight may have changed resulting in a somewhat different frontal distribution pattern. A breakdown of the summer stratification pattern within the bight in the month of September was reported during a 1976 experiment (Becker *et al.* 1979). None the less, both data sets indicate that mixing within the German Bight is much more complex than previously presumed, occurring in a broad zone across the bight, and persisting seaward of the inner bight region.

6. Conclusions

The data obtained by the NASA AOL during investigations conducted in conjunction with the MARSEN ocean fronts experiments with a U.V. laser indicate that synoptic maps of water clarity and dissolved organic fluorescence can be obtained for moderate size estuaries. Despite some calibration problems associated with the AOL fluorosensor (since corrected), data of sufficient quality were obtained

to permit the tracing of major watermasses throughout the portion of the bight landward of Helgoland. The general distribution patterns of these watermasses obtained from the AOL data is in reasonable agreement with published results obtained using conventional as well as other remote sensing techniques. Finally, Gelbstoff fluorescence after normalization with Raman backscatter signal can be utilized to define and measure estuarine frontal features within certain constraints provided source areas for the fluorescing, dissolved organic materials within the estuary can be defined. The resulting composites of estuarine fronts obtained during two flight experiments over the German Bight indicate that mixing within the bight is more complex than previously reported prior to the MARSEN experiment. Areas of mixing are strongest both north and east of the entrance of the Elbe and Weser Rivers and mixing persists seaward of the island of Helgoland. Comparison of these frontal maps with those produced by the German scientists using shipborne instrumentation earlier in the MARSEN experiment is difficult due to the lack of common coverage.

Modifications made to the AOL fluorosensor since the 1979 MARSEN experiments promise to allow improved resolution and extendability for airborne measurement of estuarine frontal features. These instrumentation changes include the addition of an excimer pumped dye laser system and a software controllable voltage supply for the individual fluorosensor PMTs. Alterations in the AOL optics and software allow the acquisition of spectral data excited by the excimer laser at wavelengths of 308, 337·1 and 351·1 nm or from the dye laser at various visible wavelengths on alternating pulses with a 532·1 nm frequency doubled Nd:YAG laser. This combination would allow measurement of chlorophyll *a* and other organic pigments associated with photoplankton as well as the Gelbstoff fluorescence obtained during these experiments. The additional Raman from the blue–green laser would facilitate improved spectral correction for water optical attenuation properties across the entire spectrum. The individual voltage controls for the fluorosensor PMTs have already demonstrated that 'cleaner' spectra can be obtained with improved calibration. These spectra are of sufficient quality to allow standard interpolation techniques (Kung and Itzkan 1976) to be utilized for removal of Gelbstoff fluorescence from the Raman backscatter band.

Acknowledgments

No experiment of this magnitude could be executed without the assistance of numerous scientists and engineers to whom we are indebted. Specifically, we wish to thank Omar Shemdin and James Blue for the scientific and logistical project coordination.

References

Becker, G. A., Carlson, H., and Kempe, P., 1979, *Deutsche Bucht: Hydrographie, Stromung, Seegang* (Deutsches Hydrographic Institut Nr. 2149/21, Hamburg).

Becker, G., Prahm-Rodewald, G., 1980, Fronts in the Sea, salinity fronts in the German Bight, *Seewart*, **41**, 12.

Blume, H. J. C., Kendall, B. M., and Fedors, J. C., 1981, Multifrequency radiometer detection of submarine freshwater sources along the Puerto Rican coastline. *J. geophys. Res.*, **86**, 5283.

Bowman, M. J., and Esaias, W. E. (editors), 1978, *Oceanic Fronts in Coastal Processes* (New York: Springer-Verlag).

BRISTOW, M. P. F., 1978, Airborne monitoring of surface water pollutants by fluoroescence spectroscopy. *Remote Sensing Environ.*, **7**, 105.

BRISTOW, M., NIELSEN, D., BUNDY, D., and FURTEK, R., 1981, Use of water Raman emission to correct airborne laser fluorosensor data for effects of water optical attenuation. *Appl. Optics*, **20**, 2889.

GORDON, H. R., 1981, Surface water phytoplankton concentration derived from satellite measurements of ocean color. *Proceedings of the Optical Society of America*, 1981 Annual Meeting, Paper No. FP1.

HOGE, F. E., and SWIFT, R. N., 1980a, Oil film thickness measurement using airborne laser-induced water Raman backscatter. *Appl. Optics.*, **19**, 3269.

HOGE, F. E., and SWIFT, R. N., 1980b, Application of the NASA airborne oceanographic lidar to the mapping of chlorophyll and other organic pigments. *The Chesapeake Bay Plume Study*, Superflux 1980, NASA Conference Proceedings, Document No. CP2188.

HOGE, F. E., and SWIFT, R. N., 1981a, Airborne simultaneous spectroscopic detection of laser-induced water Raman backscatter and fluorescence from chlorophyll *a* and other naturally occurring pigments. *Appl. Optics*, **20**, 3197.

HOGE, F. E., and SWIFT, R. N., 1981b, Absolute tracer dye concentration using airborne laser-induced water Raman backscatter. *Appl. Optics*, **20**, 1191.

HOGE, F. E., SWIFT, R. N., and FREDERICK, E. B., 1980, Water depth measurement using an airborne pulsed neon laser system. *Appl. Optics*, **19**, 871.

HUHNERFUSS, H., ALPERS, W., and JONES, W. L., 1978, Measurements at 13·9 GHz of the radar backscattering cross section of the North Sea covered with an artificial surface film. *Radio Sci.*, **13**, 979.

HUHNERFUSS, H., ALPERS, W., JONES, W. L., LANGE, P. A., and RICHTER, K., 1981, The damping of ocean surface waves by a molecular film measured by wave staffs and microwave radars. *J. Geophys. Res.*, **86**, 429.

JANOPAUL, M. M., FRISCH, A. S. and LYONS, R. S., 1981, HF radar measurements of surface currents in the German Bight during MARSEN phase 2. NOAA Technical Memorandum ERL WPL–71, Wave Propagation Laboratory, Boulder, Colorado, U.S.A.

JOHNSON, J. W., WEISSMAN, D. E., and JONES, W. L., 1982, Measurements of ocean gravity wave spectrum from an aircraft using the two-frequency microwave resonance technique. *Int. J. Remote Sensing*, **3**, 383–407.

JOHNSON, R. W., and HARRISS, R. C., 1980, Remote sensing for water quality and biological measurements in coastal waters. *Photogramm. Enging Remote Sensing*, **46**, 77.

KASHA, M., 1948, Transmission filters for the ultraviolet. *J. Opt. Soc. Am.*, **38**, 929.

KLEMAS, V., and POLIS, D. F., 1977, Remote sensing of estuarine fronts and their effects on pollutants. *Photogramm. Enging Remote Sensing*, **43**, 599.

KUNG, R. T. V., and ITZKAN, I., 1976, Absolute oil fluoroscence conversion efficiency. *Appl. Optics*, **15**, 409.

O'NEIL, F. A., 1981, Field trials of a lidar bathymeter in the Magdalen Islands. *Proc. Fourth Laser Hydrography Symposium*, 30 September to 3 October 1980, Special Document No. ERL–0143–SD, Defence Research Centre, Salisbury, South Australia, Paper No. 5, p. 56.

O'NEIL, R. A., BRISTOW, M. P. F., and HOGE, F. E., 1981, The current status of airborne laser fluorosensing. *Proc. 15th Int. Symp. Remote Sensing Environ.*, Ann Arbor, Michigan.

O'NEIL, R. A., BUJA-BIJUNAS, L., and RAYNER, D. M., 1980, Field performance of a laser fluorosensor for the detection of oil spills. *Appl. Optics*, **19**, 863.

PENNY, M. F., and PHILLIPS, D. M., (editors), 1981, *Proc. Fourth Laser Hydrography Symposium*, 30 September to 3 October 1980, Special Document No. ERL–0143–SD, Defence Research Centre, Salisbury, South Australia.

SWIFT, C. T., 1980, Passive microwave remote sensing of the ocean-A review. *Bound. Layer Met.*, **18**, 25.

ZIMMERMAN, A. V., PAUL, F. W., and EXTON, R. J., 1976, Research and investigation of the radiation induced by a laser beam incident on sea water. Contractor Final Report CR–14519, NASA Grant NSA–1096, Chesapeake College, Wye Mills, Maryland, U.S.A.